Chapter 4
Multilayer Silicene

Silicon does not have a naturally occurring layered allotrope like graphite. However, it is possible to grow monolayer silicene on substrates, as we have seen in Chap. 3. Extending this idea further, one may wonder whether it is possible to synthesize layered silicon structures by continuing the growth started as a monolayer silicene. In this chapter we discuss the experimental and theoretical works that are based on this idea of multilayer silicene growth.

4.1 Experimental Evidence

When Si deposition is prolonged beyond the formation of the first layer 3×3/4×4 or $\sqrt{7} \times \sqrt{7}/\sqrt{13} \times \sqrt{13}$ phases and in the same conditions, growth of multilayer silicene, which possesses a unique $\sqrt{3} \times \sqrt{3}$R(30°) (in short $\sqrt{3} \times \sqrt{3}$) structure is obtained. Such films grow in successive terraces, each showing this unique reconstruction. If growth occurs on the prototype 3×3/4×4 phase, one gets a single orientation of these terraces. Instead, if growth occurs on the initial $\sqrt{7} \times \sqrt{7}/\sqrt{13} \times \sqrt{13}$ first layer silicene phase, rotated terraces are obtained; the rotation angles are directly related to those of the first layer domains (Salomon et al. 2014). In angle-resolved photoemission (ARPES) measurements, these films possess a Dirac cone at the centre of the Brillouin zone due to back folding of the $\sqrt{3} \times \sqrt{3}$ silicene superstructure with a Fermi velocity about half that of the free standing graphene (De Padova et al. 2013a,b). Vogt et al. have studied terraces with up to five layers of $\sqrt{3} \times \sqrt{3}$ silicene. They have shown that the height difference between adjacent terraces is ∼3.1 Å (Vogt et al. 2014). Using in situ a four probe scanning tunneling microscope, a sheet resistance analogous to that of thin films of graphite in nano-grains was determined. De Padova et al. took this even further and synthesized few tens monolayers of silicene with $\sqrt{3} \times \sqrt{3}$ reconstruction.

S. Cahangirov et al., *Introduction to the Physics of Silicene and other 2D Materials*, Lecture Notes in Physics 930,
DOI 10.1007/978-3-319-46572-2_4

Remarkably, these multilayer silicene films survive after exposure in ambient air for a day at least, because just the very top layers are oxidized; the film underneath remains intact, as directly revealed via a graphite-like Raman signature (De Padova et al. 2014). Feng et al. have investigated bilayers of $\sqrt{3} \times \sqrt{3}$ silicene (Feng et al. 2012). They have measured the quasi-particle interference of electrons in the first layer due to the scattering from the islands formed by the second layer grown on top (Chen et al. 2012). A linear dispersion with high Fermi velocity was derived from these interference patterns.

4.2 Atomic Structure

Although multilayer silicene was grown in many experiments mentioned above its atomic structure has been a subject of debate. The experiments report a 5 % contracted $\sqrt{3} \times \sqrt{3}$ structure that has a honeycomb appearance in STM imaging with a $\sim$3.1 Å distance between its layers. However, there is still no structural model that explains all these observations. Here we discuss the proposed models and point out their shortcomings.

The interlayer separation of multilayer silicene is very close but measurably different from that of Si(111). This inspired models of multilayer silicene that has bulk silicon-like interior with a modified surface structure. One such model is based on the Si(111)-Ag$\sqrt{3} \times \sqrt{3}$ system also mentioned in Chap. 3. The various surfaces obtained by the deposition of Ag on Si(111) substrate were studied intensively in the 1980s (Lelay et al. 1978; van Loenen et al. 1987; Vlieg et al. 1989; Ding et al. 1991). One of the most favorable surfaces that were observed in experiments was the so called honeycomb-chain trimer (HCT) structure (Vlieg et al. 1989). As seen in Fig. 4.1, the HCT model has a $\sqrt{3} \times \sqrt{3}$ honeycomb STM pattern that resembles the one observed in multilayer silicene experiments. Furthermore, the interlayer separation is close to the one obtained in experiments since the bulk region is basically Si(111). The HCT structure makes transition to the so-called inequivalent triangle (IET) structure at low temperatures. This transition could explain the spontaneous symmetry breaking observed in $\sqrt{3} \times \sqrt{3}$ silicene at low temperatures (Chen et al. 2013; Shirai et al. 2014). Finally, it was argued that the slope of the linear portion of the S_1 band formed by the Si(111)-Ag$\sqrt{3} \times \sqrt{3}$ surface is comparable to that of the linear bands observed in $\sqrt{3} \times \sqrt{3}$ silicene experiments (Sato et al. 1999; Chen et al. 2012; Shirai et al. 2014). However, the HCT model does not account for the contraction of the lattice constant observed in experiments. Another model inspired by the bulk silicon structure is the tristable Si(111) bilayer grown on Ag substrate (Guo and Oshiyama 2014). As mentioned in Chap. 3, the flip-flop motion that is suggested to give rise to the honeycomb STM topographs is not supported by convincing arguments. Also it does not explain the lattice contraction and can not be extended to multilayers.

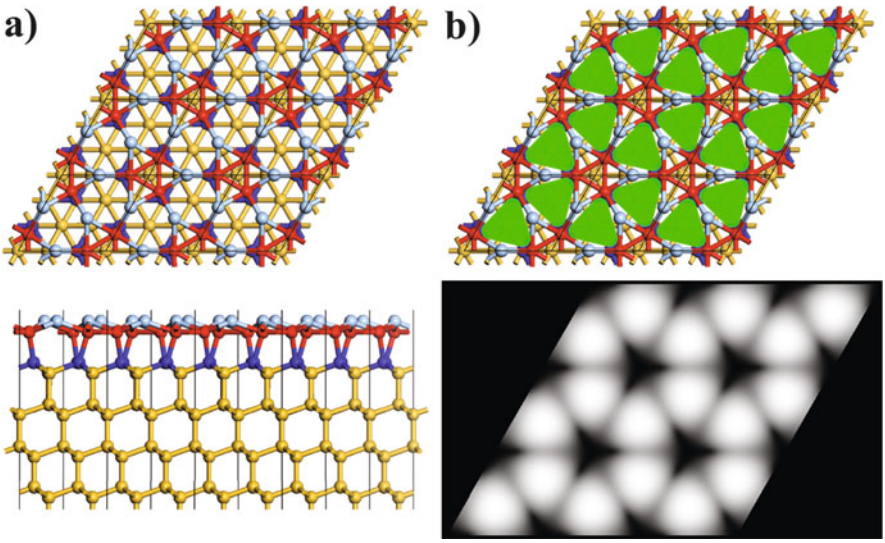

Fig. 4.1 (**a**) Ball and stick representation of the honeycomb-chain trimer (HCT) model (Vlieg et al. 1989). The top and side views are presented in the *top* and *bottom* panels, respectively. The *yellow balls* are Si atoms sitting in almost ideal positions of the Si(111) substrate. The topmost layer of Si atoms and the layer below them are represented by the *red* and the *blue balls*, respectively. The Ag atoms represented by the *light blue balls* form the topmost atomic layer of the system by attaching to Si atoms (*red balls*) below them. (**b**) Schematic and calculated STM image of HCT structure are presented in *top* and *bottom panels*, respectively. The *bright triangular spots* that are observed in the STM image are represented by *green triangles* superimposed on the top view of the ball and stick model

4.3 Silicites

Here we present a possible growth model of multilayer silicene that produces structures which are in a good agreement with experiments (Cahangirov et al. 2014). A realistic growth simulation is really hard to do because one needs to take into account many experimental parameters. It is especially hard to run a molecular dynamics simulation long enough for the atoms to explore the whole energy landscape. Instead, we present structural relaxations accompanied with educated guesses.

A silicene monolayer is first placed on top of the already formed HDS structure, as seen in Fig. 4.2. Upon relaxation of this system, one of the dumbbell atoms in HDS transfers to the silicene layer forming a dumbbell unit there. As a result, HDS loses one dumbbell unit and becomes TDS, while silicene sheet gains one dumbbell unit and also becomes TDS. The two TDS layers become connected to each other by covalent bonds. However, the number and strength of these vertical covalent bonds are less compared to the ones formed between two (111) planes of cubic diamond silicon (cdSi).

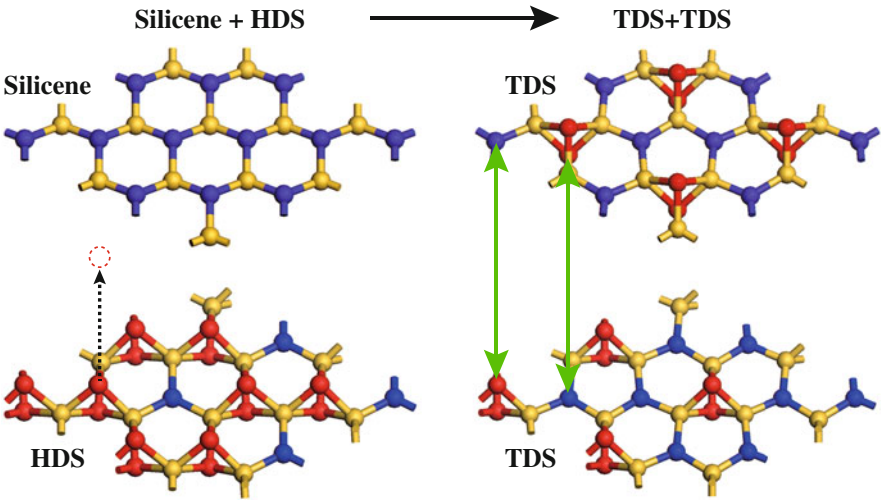

Fig. 4.2 A possible growth mechanism of multilayer silicene or silicites. When silicene is put on top of HDS, one of the dumbbell atoms transfer to the silicene layer, as shown by *dashed black arrow*. As a result, two TDS layers are formed, that connect to each other through covalent bonding between atoms shown by *green arrows*

If we continue depositing Si atoms onto the bilayer TDS system, the TDS layer on top will first transform to HDS. This HDS layer will follow the same faith as the original HDS structure, transforming itself to TDS by donating one dumbbell to create another TDS on top, which in turn will transform to yet another HDS layer. This process will continue producing multiple TDS layers connected to each other with an HDS layer on the very top. This is in agreement with experiments that continue to see the $\sqrt{3} \times \sqrt{3}$ honeycomb pattern in the STM measurements performed on multilayer silicene. It is possible to stack TDS layers in eclipsed or staggered fashion, as shown in Fig. 4.3a. The resulting bulk structures are named eclipsed (eLDS) and staggered (sLDS) layered dumbbell silicite, accordingly. All atoms in both eLDS and sLDS structure are fourfold coordinated. However, the covalent bonds significantly deviate from the ideal tetrahedral bonding angle of 109°. In the eLDS structure the TDS layers are just shifted by one third of their 2D unitcell vectors and stacked on top of each other. As shown in Fig. 4.3a, stacking follows ABCABC…and so on. It cannot be ABABAB…because in that case blue atoms would be connected to dumbbell atoms from both sides, which would unfavorably increase their coordination from four to five. The stacking of the sLDS structure is similar, but the layers are staggered with respect to each other. This is represented by a bar on top of the staggered layers.

Both eLDS and sLDS are open structures similar to the structure of cubic silicon. In fact, the mass densities of eLDS (2.10 g/cm^3) and sLDS (2.11 g/cm^3) are smaller than that of cdSi (2.28 g/cm^3). The interlayer distance in both eLDS and sLDS structures are around 4.3 Å. This is in contrast to experiments that find the interlayer

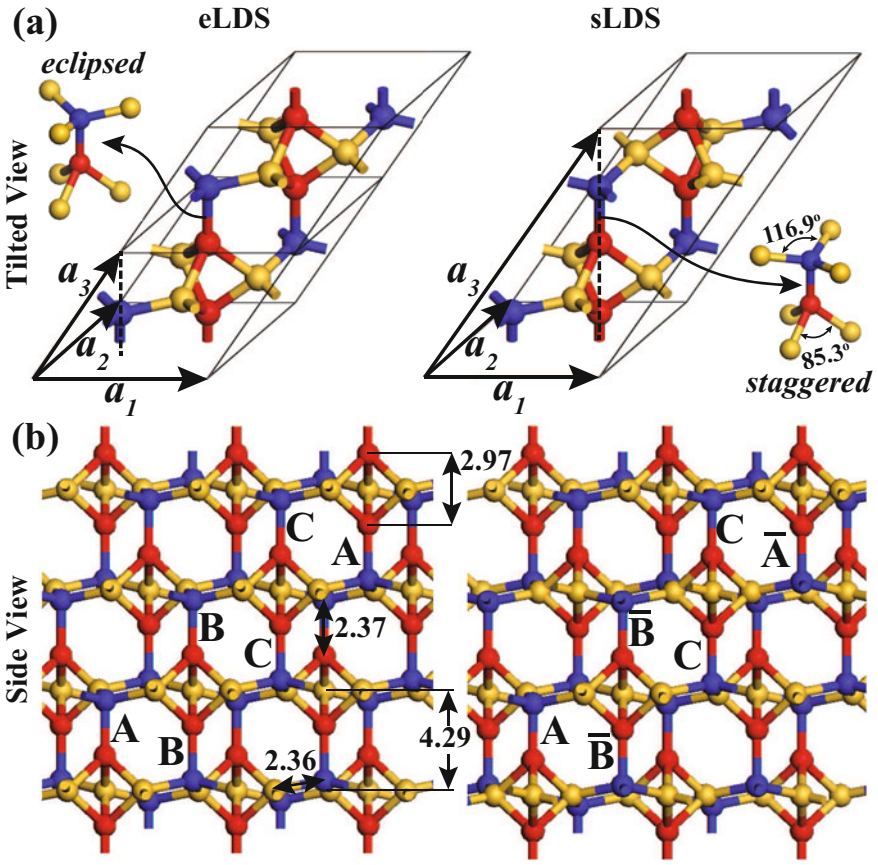

Fig. 4.3 (**a**) The double unit cell of eclipsed layered dumbbell silicite (eLDS) including N=7 Si atoms per unit cell and single unit cell of staggered layered dumbbell silicite (sLDS) including N=14 Si atoms per unit cell. (**b**) Side view showing the ABCABC... stacking of eLDS and the $A\bar{B}C\bar{A}B\bar{C}A$... stacking of sLDS. The bond lengths are given in Angström (Cahangirov et al. 2014)

distance to be 3.1 Å. Further work needs to be done to resolve this disagreement between theory and experiment. Due to the covalent bonds connecting LDS layers, the interlayer interaction is not like the weak van der Waals interaction found in graphite or MoS_2. However, these covalent bonds are sparse compared to those found between Si(111) layers in cubic silicon. The calculated cohesive energies are 4.42 and 4.43 eV per atom for eLDS and sLDS, respectively which is very close to that of cdSi (4.60 eV).

The calculated vibrational frequencies of eLDS and sLDS phases are all found to be positive. The absence of negative frequencies is taken as an evidence that these layered phases are stable. The phonon bands of these structures presented in Fig. 4.4 disclose interesting dimensionality effects. Specific optical branches are

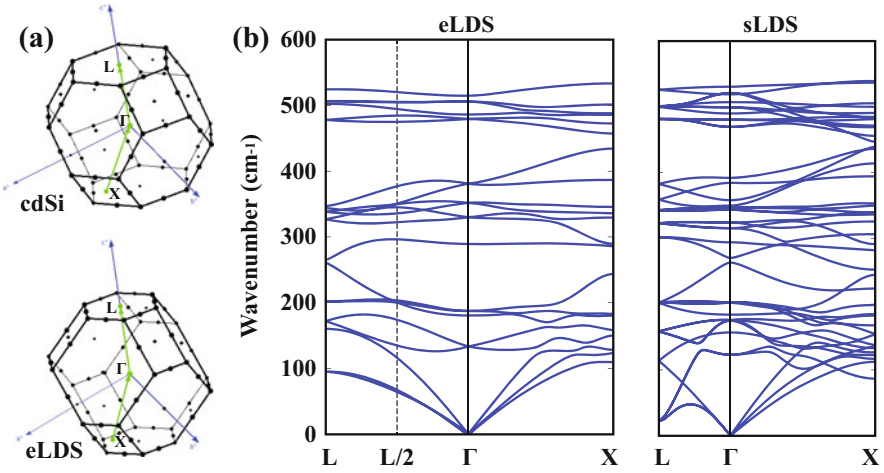

Fig. 4.4 (**a**) Brillouin Zones of cdSi and eLDS with relevant symmetry directions. (**b**) Phonon bands of eLDS and sLDS

flat and the lower lying branches overlap with the acoustical branches. One of the acoustical branches of the sLDS structure dips in near the point L, indicating phonon softening. We have also performed molecular dynamics simulations where (3×3×4) supercells of eLDS and (3×3×2) supercells of sLDS were kept at 1000 K for 4 ps. No structural deformation was observed in the course of these simulations, which corroborates the stability of these materials.

The layered character of eLDS and sLDS can be conveniently substantiated by investigating the in-plane and out of plane Young modulus and by comparing them with those of cdSi. The perpendicular Young's moduli of eLDS and sLDS are calculated as $Y_{\perp}$=79.6 GPa and 76.4 GPa, respectively, while the Young's modulus of cdSi along [111] direction is 176.0 GPa and hence more than twice the value of LDS phases. In contrast, the in-plane Young's modulus calculated within TDS layers of eLDS and sLDS are relatively higher, and are 176.3 GPa and 161.9 GPa, respectively. These values are comparable with the Young's modulus of cdSi calculated in the (111) plane, which is 200 GPa. The dramatic differences between the Young's modulus of LDS structures and that of cdSi calculated in the direction perpendicular to the layers confirm the layered nature of eLDS and sLDS phases.

The electronic structures of eLDS and sLDS phases have indirect band gaps, which are wider than that of cdSi, as shown in Fig. 4.5a. The calculated indirect (direct) band gaps of eLDS and sLDS are 0.98 (1.43) eV and 1.26 (1.65) eV, respectively. The indirect band gap of cdSi is 0.62 eV at the DFT-PBE level while it is increased to 1.12 eV upon including many-body self-energy corrections at the G_0W_0 level (Hedin 1965; Shishkin and Kresse 2007). With G_0W_0 correction the indirect band gap of eLDS increased to 1.52 eV. Indirect (direct) band gaps of eLDS

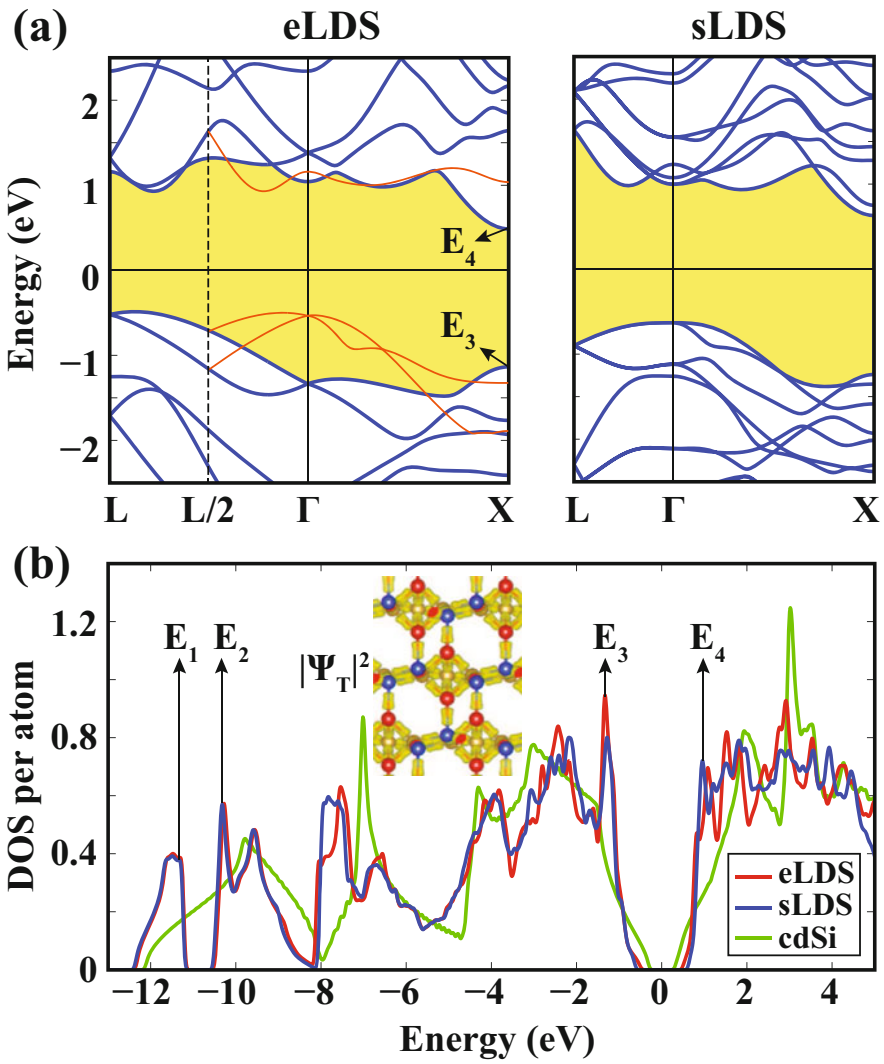

Fig. 4.5 (**a**) Energy band structure of eLDS and sLDS. Zero of energy is set to the Fermi level. Bands of eLDS folded by doubling the unit cell along a_3 are shown by *red lines*. (**b**) Normalized densities of states (DOS) of eLDS, sLDS and cdSi. The isosurfaces of the total charge density shown by inset confirm the layered nature

and sLDS calculated by HSE06 hybrid functional are 1.92 eV (2.37 eV) and 1.88 eV (2.26 eV), respectively.

Owing to the different Brillouin zones it is difficult to directly compare the band structures of LDS and cdSi. Therefore, the effects of the layered character on the electronic structure are sought in the normalized densities of states (DOS).

Figure 4.5b shows the normalized DOSs of eLDS, sLDS and cdSi. Except for some peak shifts, the DOSs of silicites are similar. Owing to the fourfold coordination of Si atoms in all structures, the overall features of DOSs of LDS structures appear to be reminiscent of that of cdSi. This confirms the fact that the overall features of the bands of cdSi can be obtained within the first nearest neighbor coupling (Harrison and Ciraci 1974). The total charge density, $|\Psi_T|^2$ presented by inset, depicts that electrons are mainly confined to TDS layers. This is another clear manifestation of the layered character of eLDS and sLDS phases. On the other hand, significant differences are distinguished in the details of the electronic energy structures due to deviations from tetrahedral coordination: (1) Indirect band gaps relatively larger than that of cdSi can offer promising applications in micro and nanoelectronics. (2) Sharp peaks E_3 and E_4 near the edges of the valence and conduction bands, originate from the states, which are confined to TDS layers and can add critical functionalities in optoelectronic properties. (3) A gap opens near the bottom of the valence band at ~ -11 eV; its edge states are also confined to TDS layers.

The in-plane and out of plane static dielectric responses also reflect the layered nature of silicite. As a matter of fact, the calculated in-plane dielectric constant of eLDS (sLDS) is $\epsilon_{\parallel}$=12.52 (12.85), while its out of plane dielectric constant is $\epsilon_{\perp}$=11.69 (11.56). Those values are contrasted with the uniform dielectric constant, ϵ=12.19 of cdSi. In Fig. 4.6 we present the optical absorption spectra of eLDS and cdSi calculated at the RPA level using the Kohn-Sham wave functions and G_0W_0 corrected eigenvalues. The frequency dependent dielectric matrix takes different values in the in-plane and out of the plane directions of eLDS while for cdSi it is isotropic. One can see that the optical absorption of eLDS is significantly enhanced in the visible range compared to cdSi which makes it a potential candidate material for photovoltaic applications. This enhancement is still present when we rigidly shift the absorption spectra by the amount we get from G_0W_0 corrections (Onida et al. 2002).

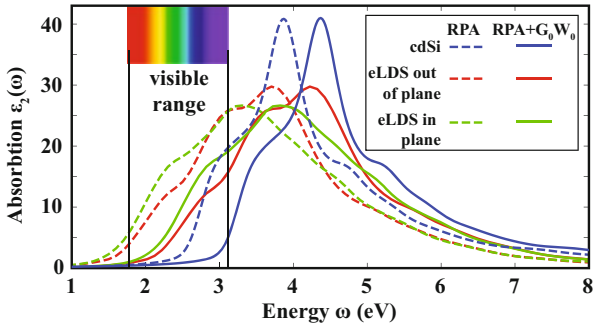

Fig. 4.6 The calculated Kohn-Sham and G_0W_0 RPA optical absorption spectra for eLDS and cdSi

References

Cahangirov, S., Özçelik, V.O., Rubio, A., Ciraci, S.: Silicite: the layered allotrope of silicon. Phys. Rev. B **90**, 085426 (2014)

Chen, L., Liu, C.C., Feng, B., He, X., Cheng, P., Ding, Z., Meng, S., Yao, Y., Wu, K.: Evidence for Dirac fermions in a honeycomb lattice based on silicon. Phys. Rev. Lett. **109**, 056804 (2012)

Chen, L., Li, H., Feng, B., Ding, Z., Qiu, J., Cheng, P., Wu, K., Meng, S.: Spontaneous symmetry breaking and dynamic phase transition in monolayer silicene. Phys. Rev. Lett. **110**, 085504 (2013)

De Padova, P., Avila, J., Resta, A., Razado-Colambo, I., Quaresima, C., Ottaviani, C., Olivieri, B., Bruhn, T., Vogt, P., Asensio, M.C., Lay, G.L.: The quasiparticle band dispersion in epitaxial multilayer silicene. J. Phys. Condens. Matter **25**, 382202 (2013a)

De Padova, P., Vogt, P., Resta, A., Avila, J., Razado-Colambo, I., Quaresima, C., Ottaviani, C., Olivieri, B., Bruhn, T., Hirahara, T., Shirai, T., Hasegawa, S., Carmen Asensio, M., Le Lay, G.: Evidence of Dirac fermions in multilayer silicene. Appl. Phys. Lett. **102**, 163106 (2013b)

De Padova, P., Ottaviani, C., Quaresima, C., Olivieri, B., Imperatori, P., Salomon, E., Angot, T., Quagliano, L., Romano, C., Vona, A., Muniz-Miranda, M., Generosi, A., Paci, B., Lay, G.L.: 24 h stability of thick multilayer silicene in air. 2D Mater. **1**, 021003 (2014)

Ding, Y.G., Chan, C.T., Ho, K.M.: Structure of the $(\sqrt{3} \times \sqrt{3})$ $R30°$ Ag/Si(111) surface from first-principles calculations. Phys. Rev. Lett. **67**, 1454–1457 (1991)

Feng, B., Ding, Z., Meng, S., Yao, Y., He, X., Cheng, P., Chen, L., Wu, K.: Evidence of silicene in honeycomb structures of silicon on Ag(111). Nano Letters **12**, 3507–3511 (2012)

Guo, Z.X., Oshiyama, A.: Structural tristability and deep Dirac states in bilayer silicene on Ag(111) surfaces. Phys. Rev. B **89**, 155418 (2014)

Harrison, W.A., Ciraci, S.: Bond-orbital model II. Phys. Rev. B **10**, 1516–1527 (1974)

Hedin, L.: New method for calculating the one-particle Green's function with application to the electron-gas problem. Phys. Rev. **139**, A796–A823 (1965)

Lelay, G., Manneville, M., Kern, R.: Cohesive energy of the two-dimensional Si(111) 3×1 Ag and Si(111)$\sqrt{3}$-R(30°) Ag phases of the silver (deposit)-silicon(111) (substrate) system. Surf. Sci. **72**, 405–422 (1978)

Onida, G., Reining, L., Rubio, A.: Electronic excitations: density-functional versus many-body Green's-function approaches. Rev. Mod. Phys. **74**, 601–659 (2002)

Salomon, E., Ajjouri, R.E., Lay, G.L., Angot, T.: Growth and structural properties of silicene at multilayer coverage. J. Phys. Condens. Matter **26**, 185003 (2014)

Sato, N., Nagao, T., Hasegawa, S.: Si(111)-($\sqrt{3} \times \sqrt{3}$)-Ag surface at low temperatures: symmetry breaking and surface twin boundaries. Surf. Sci. **442**, 65–73 (1999)

Shirai, T., Shirasawa, T., Hirahara, T., Fukui, N., Takahashi, T., Hasegawa, S.: Structure determination of multilayer silicene grown on Ag(111) films by electron diffraction: evidence for Ag segregation at the surface. Phys. Rev. B **89**, 241403 (2014)

Shishkin, M., Kresse, G.: Self-consistent GW calculations for semiconductors and insulators. Phys. Rev. B **75**, 235102 (2007)

van Loenen, E.J., Demuth, J.E., Tromp, R.M., Hamers, R.J.: Local electron states and surface geometry of Si(111)-$\sqrt{3} \times \sqrt{3}$ Ag. Phys. Rev. Lett. **58**, 373–376 (1987)

Vlieg, E., Gon, A.V.D., Veen, J.V.D., MacDonald, J., Norris, C.: The structure of Si(111)-($\sqrt{3} \times \sqrt{3}$)r30°-Ag determined by surface X-ray diffraction. Surf. Sci. **209**, 100–114 (1989)

Vogt, P., Capiod, P., Berthe, M., Resta, A., De Padova, P., Bruhn, T., Le Lay, G., Grandidier, B.: Synthesis and electrical conductivity of multilayer silicene. Appl. Phys. Lett. **104**, 021602 (2014)